



January 2015

Iridium Modified Silicon (001) Surface

Sehtab Hossain

Follow this and additional works at: <https://commons.und.edu/theses>

Recommended Citation

Hossain, Sehtab, "Iridium Modified Silicon (001) Surface" (2015). *Theses and Dissertations*. 1785.
<https://commons.und.edu/theses/1785>

This Thesis is brought to you for free and open access by the Theses, Dissertations, and Senior Projects at UND Scholarly Commons. It has been accepted for inclusion in Theses and Dissertations by an authorized administrator of UND Scholarly Commons. For more information, please contact zeinebyousif@library.und.edu.

IRIDIUM MODIFIED SILICON (001) SURFACE

By

Sehtab Hossain

Bachelor of Science, Islamic University of Technology, November'2008

A Thesis

Submitted to the Graduate Faculty

Of the

University of North Dakota

In the partial fulfillment of the requirements

For the degree of

Master of Science

Grand Forks, North Dakota

August

2015

This thesis, submitted by Shtab Hossain is a partial fulfillment of the requirements for the degree of Master of Science from the University of North Dakota, has been read by Faculty Advisor Committee under whom the work has been done and hereby approved.

Saleh Faruque 08/04/15

Dr. Saleh Faruque, Chair

Nuri Oncel 08/04/15

Dr. Nuri Oncel, Co-chair

Naima Kaabouch 08/04/15

Dr. Naima Kaabouch

S. Nogharian

Dr. Sima Nogharian

This thesis meets the standards of appearance, conforms to the style and format requirements of the Graduate School of the University of North Dakota, and is hereby approved.

Wayne Swisher
August 17, 2015

Dr. Wayne Swisher, Dean of the Graduate School

PERMISSION

Title	Iridium Modified Silicon (001) Surface
Department	Electrical Engineering
Degree	Master of Science

In presenting this thesis in partial fulfillment of the requirements for a graduate degree from the University of North Dakota, I agree that the library of this University shall make it freely available for inspection. I further agree that permission for extensive copying for scholarly purposes may be granted by the professor who supervised my thesis work or, in her absence, by the chairperson of the department or the dean of the Graduate School. It is understood that any copying or publication or other use of this thesis or part thereof for financial gain shall not be allowed without my written permission. It is also understood that due recognition shall be given to me and to the University of North Dakota in any scholarly use which may be made of any material in my thesis.

Sehtab Hossain

August 7, 2015.

TABLE OF CONTENTS

LIST OF FIGURES.....	V
LIST OF TABLES.....	VI
ACKNOWLEDGEMENTS.....	VII
ABSTRACT.....	VIII
CHAPTER	
I. INTRODUCTION.....	1
II. SCANNING TUNNELING MICROSCOPY (STM).....	3
III. IRIDIUM MODIFIED SILICON (001) SURFACE.....	15
IV. CONCLUSION.....	30
REFERENCES.....	32

LISTS OF FIGURES

Figure	Page
2.1 The Schematic of a STM System.....	4
2.2 Block Diagram of a STM System.....	5
2.3 Potential Barrier and propagation directions of the incident reflected and transmitted wave.	8
2.4 Potential For Vacuum Barrier for two electrodes.....	10
3.1 Silicon Crystal and Surface.....	15
3.2 Top View Of Different Si(001) Surfaces.....	16
3.3 Zoomed Clean Silicon Surface.....	17
3.4 Zoomed in frame 30nm x 30nm Silicon (001) Surface.....	19
3.5 Length vs Island number histogram for 0.25 ML.....	22
3.6 Length vs Island number histogram for 0.5 ML.....	23
3.7 Width vs Island number histogram for 0.25 ML.....	24
3.8 Width vs Island number histogram for 0.5 ML.....	25
3.9 dI/dV vs Sample Bias (V) Curve from I(V) Spectroscopy.....	27
3.10 $\ln I$ vs z Curve from Bulk Si(001), 0.25 ML and 0.5 ML Si(001) Surface.....	28

LISTS OF TABLES

Table	Page
1. Table of Width, Length, Height, W/L Ratio and Coverage of Iridium Islands.....	20
2. Correlation Analysis.....	26

ACKNOWLEDGEMENTS

I thank all who are in one way or another contributed in completion of this thesis. First I am thankful to God Almighty for His protection and grace.

I would like to express my deep gratitude to my Thesis Committee Drs. Saleh Faruque, Nuri Oncel, Naima Kaabouch and Sima Noghalian. I am very grateful for their hard work in commenting on my thesis and advise which they spent with their valuable time. Special thanks to my Cochair , Nuri Oncel for his help and guidance to make sure my work is well analyzed.

I also thank my fellow lab mates in Nanomaterial and Surface Physics group for stimulating discussion and their help and all the fun we have last two years.

Last but certainly not the least; I am grateful to my family for their continuous support. Without their support I cannot reach this far. I hope and pray that their sacrifice will not be in vain.

To My Parents

ABSTRACT

The purpose of this thesis is to fabricate Iridium modified Silicon (001) surface and investigate electronic and atomic configuration of the surface, and examine the characteristic of the surface.

In the first part, the modification done by fabrication on Si (001) surface is presented. This shows that after the modification significant pattern on the surface is visible which need to be examined for atomic and electronic structure.

The thesis then identifies the statistical analysis of the fabricated islands and examines correlation among them. Examination of surface including spectroscopy provides several important outcomes about the surface structure. Here the thesis draws several spectroscopy analyses to delve into the structure.

At the conclusion, this thesis did several examinations to investigate the surface and outcomes are in quite a good agreement with theoretical calculation and previous work [1, 2, 3]. This thesis hopes to extend its study on theoretical examination and make a small contribution on fabricating silicate.

CHAPTER 1

INTRODUCTION

Silicon (Si (14)) has unparalleled popularity in IC fabrication and also in transistor, MOSFET fabrication. Although the first transistor was made out of Germanium (Ge (32)), Si has become more popular than Ge. There are a couple of reasons for that. First of all, it is abundant in nature. Therefore, Si is cheaper than Ge. Si can tolerate higher temperatures in the processing and last but not the least it has stable oxide. At room temperature, Si crystal has fewer free electrons than Ge crystal which denotes Si will have much smaller Collector cut off current than Ge. The variation of Collector cut off current with temperature is less in Si compared to Ge. The structure of Ge crystals will be destroyed at higher temperature but Si crystals are not easily damaged by excess heat.

(001) and (111) are most commonly used and studied surface. Si (111) surface is popular for Quantum Dot fabrication which is an attractive candidate for memory device and electron entrapment and quantum confinement [1, 2]. Si (001) surface is quite popular in traditional device fabrication. It has been shown that alloying flat and/or vicinal Si and Ge substrates with various elements creates unique structures on various surfaces of Si and Ge.[1,2,3,4] Because of the high aspect ratio of these structures, they are called nanowires. Nanowires can be made up of various elements ranging from Bi [1] and rare-earth metals [1, 2 ,3] to transition metals [2,3]. Among those, transition metal nanowires is very unique since unlike rare-earth metals transition metals do not react with air to form insulating oxide layers. Au (gold) and Pt (platinum), the neighbors of Ir (Iridium) in the periodic table, have already been shown to form nanowires on various orientations of Si (Silicon) and Ge (Germanium) surfaces.

In this thesis, we fabricated Ir nanowire-silicide on Si (001) surface and study their physical and electrical properties. For analyzing the surface, we used Scanning Tunneling Microscopy (STM) which has ability to measure local electronic properties of the surfaces while taking atomic resolution topographic images. We used I-V spectroscopy and barrier height spectroscopy (I-z) to analyze electronic structure of Iridium-silicide nanowires and surface.

This thesis consists of four chapters. The second chapter represents the details of STM, sample preparation procedure and the discussions of I-V and I-z spectroscopy data taken from different

regions on the surface. The third chapter narrates the analysis of data, in its data from two spectroscopy will be analyzed to measure the electrical property of the modified surface. The last chapter stands for conclusion and future work.

Chapter 2

SCANNING TUNNELING MICROSCOPY (STM)

2.1 Theory of Scanning Tunneling Microscopy (STM):

Scanning Tunneling Microscope was invented by Binnig and Rohrer in 1981 and they got the Nobel Prize for this in 1986. At the beginning, the main objective of STM is to get powerful topographic images of the surfaces. Nowadays STM has evolved in such a way that it has become a powerful tool to study structural and electronic properties of surfaces [4, 5, 6]. STM is very much popular to use it as a microscope to see through the metal or semiconductor surface.

A typical STM consists of a sharp probing tip (usually made of Tungsten), a piezoelectric scanning unit which controls vertical and lateral movement of the tip; a coarse positioning unit which gets the tip-sample separation within the tunneling range (\sim nm); a vibration isolation stage and a set of electronics for detecting tunneling current (\sim 10pA- 1nA), and controlling the piezo-tube scanner.

In STM, when a metallic tip is brought near the close proximity of a conducting surface, electrons tunnel through the tip to the surface or vice versa. The tunneling probability and tunneling current depend exponentially on tip-sample separation. During scanning the voltage and current are kept constant by adjusting the tip-sample separation. The up-down movement of the tip is recorded as the topography of the image. The exponential dependence of the tunneling current to the tip sample separation makes it possible to measure atomic resolution. Figure.2.1 depicts the schematic diagram of a STM system [7, 8, 9].

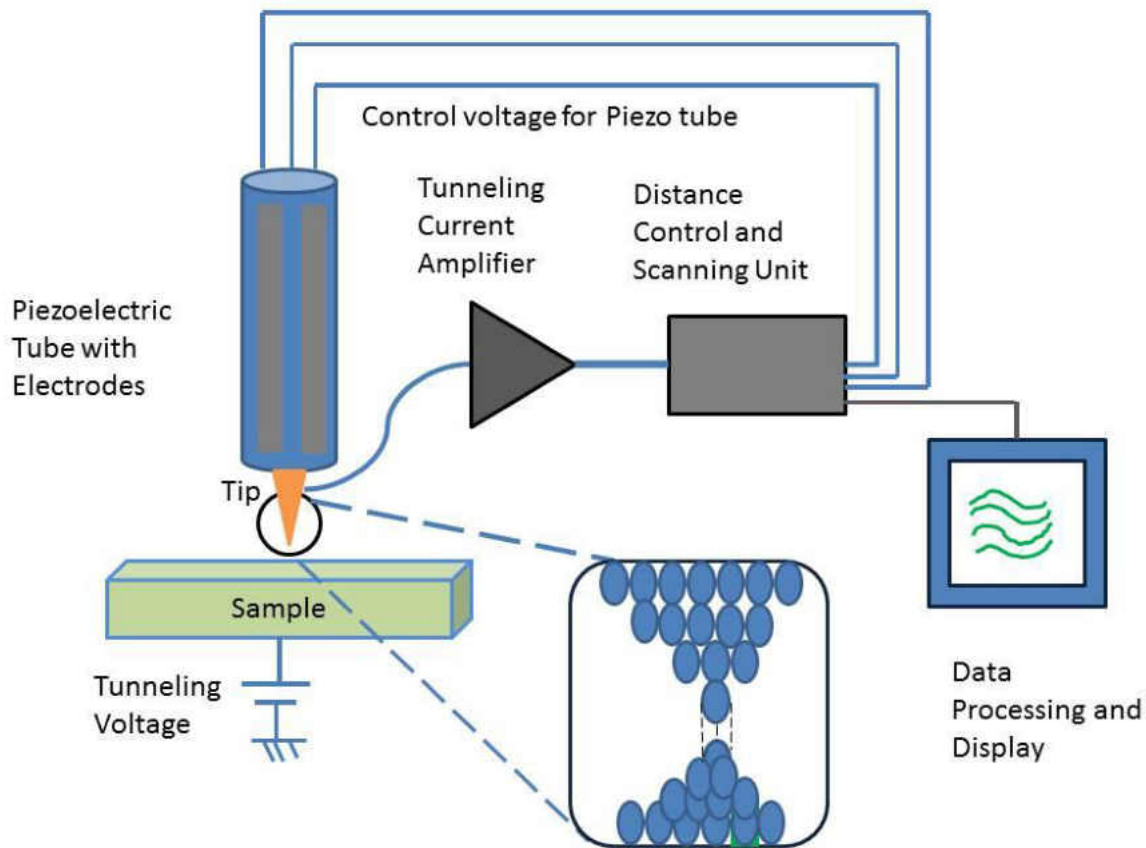


Figure 2.1: The schematic diagram of a STM system. The tip scan over the sample with a very little distance which causes the tunneling current to flow and data processing takes place and display occurs [1]

Figure 2.2 denotes the block diagram of a STM system. STM feedback control takes the output signal from current pre-amplifier and compares the signal level with a preset value, computes the response according to user defined parameter and sends voltage feedback to an analog to digital converter which is followed by a high voltage amplifier to magnify the signal to drive the piezo scanner. Controllers communicate with the computer to change bias voltage, tunneling current set point, scanning range, scanning speed and proportional/integral (PI) gain for the feedback algorithm. It also sends feedback signal and tunneling current signal to show topographic image and spectra.

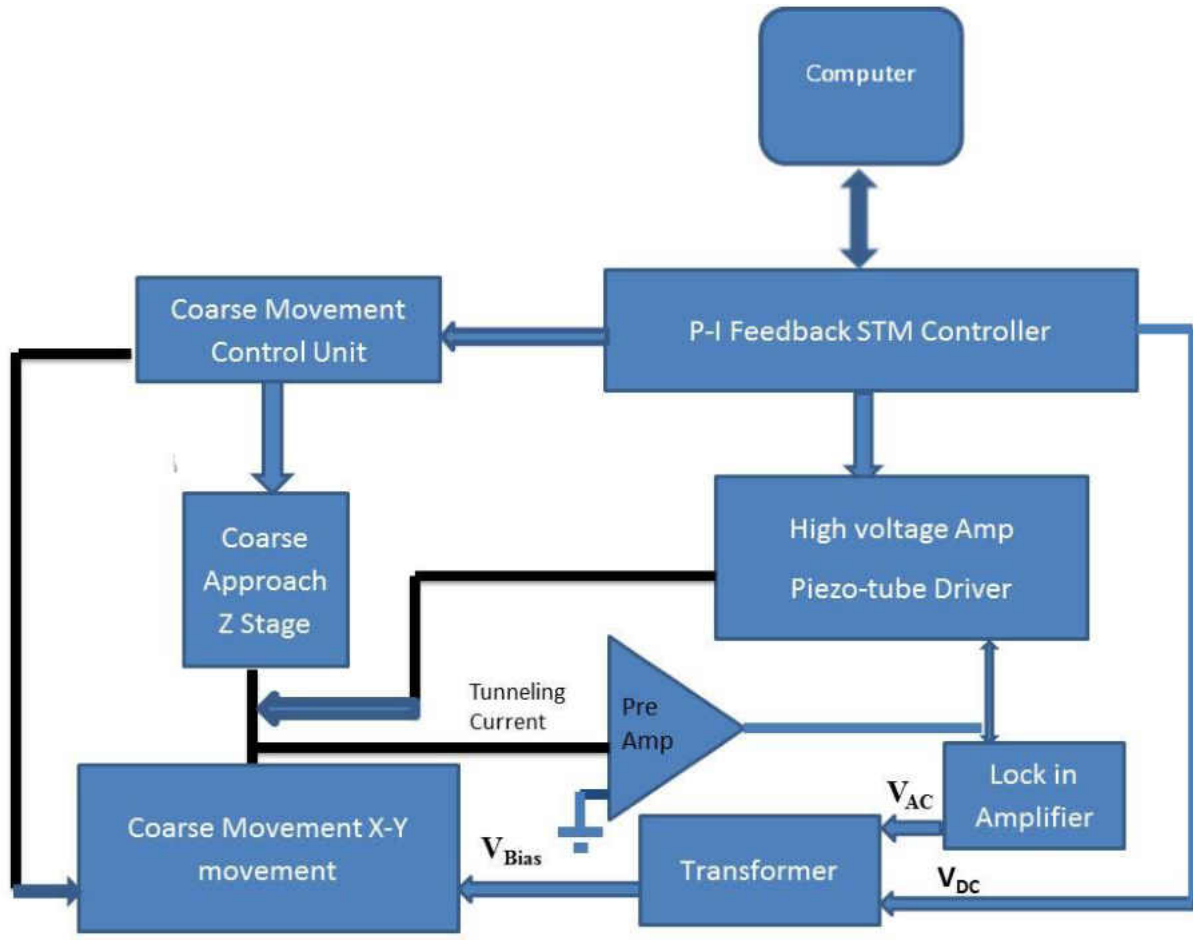


Figure 2.2: Block diagram of a STM system. Arrows denote command and travelling direction. The feedback controller, current pre-amplifier, high voltage amplifier, transformer and Lock-in amplifier make the whole STM system. [2]

2.1.1 Basic Principles:

2.1.1.1 Vacuum Tunneling:

In vacuum tunneling, the vacuum functions as a barrier between two metal electrodes. For the case of STM, the two electrodes are tip and the sample. This barrier is shown in schematic in Figure: 2.3. The transmission probability, T in a barrier in one dimension can be easily calculated. For the case of STM, we need very weak transmission for the most common range of barrier heights and widths. The state of same electron can be described by wave function, $\Psi(z)$ which will satisfy Schrödinger equation:

$$\left(\frac{-\hbar^2}{2m}\right)\frac{d^2}{dz^2}\Psi(z) + U(z)\Psi(z) = E \Psi(z) \quad (1)$$

Where \hbar is the Planck's constant (6.626×10^{-34} J-s), m is mass of electron $U(z)$ is potential energy.

To illustrate this situation we see that it is a scattering problem. We will consider a particle scattered by a potential barrier. We will investigate a particle with energy E interacting with a potential $V(z)$ and we see that the particle will first face with barrier, some particle will penetrate through the barrier and some will exit from the barrier. In this case we have three Schrödinger equations for three regions: Region I, Region II and Region III. As the barrier is stationary and does not vary with time one can perform separation of variables and time independent Schrodinger equation for Region I and III [10]:

Let us consider a beam of particles with kinetic energy E and mass m is approaching a potential barrier from the left. Potential barrier has potential V_B . In this case we will see three scenarios:

$$\begin{aligned} V(x) &= 0, \text{ when } z < 0 \\ V(x) &= V_B, \text{ when } 0 < z < a \\ V(x) &= 0, \text{ when } z > a \end{aligned} \quad (2)$$

For this case we will divide the barrier in three regions and for three regions we will get three wave functions:

In region I when $z < 0$

$$-\frac{\hbar^2}{2m} \frac{d^2}{dz^2} \Psi_1 = E \Psi_1 \quad (3)$$

In region II when $0 < z < a$

$$-\frac{\hbar^2}{2m} \frac{d^2}{dz^2} \Psi_2 + (V_B - E) \Psi_2 = E \Psi_2 \quad (4)$$

In region III when $z > a$

$$-\frac{\hbar^2}{2m} \frac{d^2}{dz^2} \Psi_3 = E \Psi_3 \quad (5)$$

After solving these three Schrodinger equations we get:

$$\Psi_1(z) = A e^{i\kappa_1 z} + B e^{-i\kappa_1 z} \quad \text{when } z < 0$$

$$\Psi(z) = \Psi_2(z) = C e^{\kappa_2 z} + D e^{-\kappa_2 z} \quad \text{when } 0 < z < a \quad (6)$$

$$\Psi_3(z) = E e^{i\kappa_1 z} \quad \text{when } z > a$$

where $\kappa_1 = \sqrt{\frac{2mE}{\hbar^2}}$ and $\kappa_2 = \sqrt{\frac{2m(V_B - E)}{\hbar^2}}$ and A, B, C, D and E are unknown coefficients.

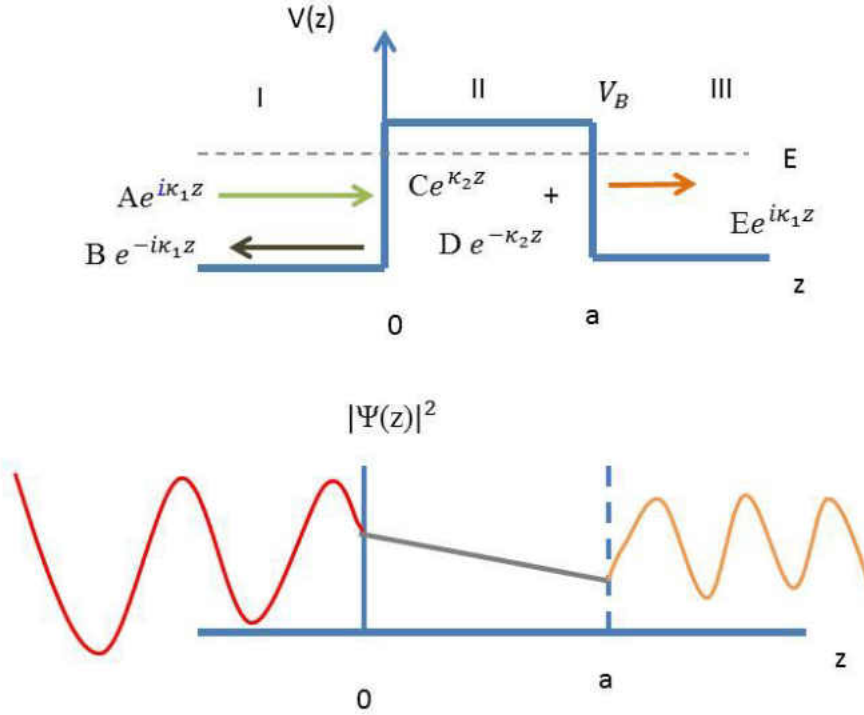


Figure 2.3: Potential barrier and propagation directions of the incident, reflected, and transmitted waves and their probability densities $|\Psi|^2$ when $E < V_B$.

The behavior of the probability density corresponding to this wave function is expected to be oscillatory in regions $z < 0$ and $z > a$ and exponentially decaying for $0 < z < a$

The continuity conditions of the wave function and its derivative at $z=0$ and $z=a$ yield:

$$A + B = C + D \quad (7)$$

$$i\kappa_1(A-B) = i\kappa_2(C-D) \quad (8)$$

$$C e^{\kappa_2 a} + D e^{-\kappa_2 a} = E e^{i\kappa_1 a} \quad (9)$$

$$\kappa_2(Ce^{\kappa_2 a} - D e^{-\kappa_2 a}) = i\kappa_1 E e^{i\kappa_1 a} \quad (10)$$

Equations 9 and 10 lead to the following expression for C and D

$$\begin{aligned} C &= \frac{E}{2} \left(1 + i \frac{\kappa_1}{\kappa_2}\right) e^{(i\kappa_1 - \kappa_2)a} \\ D &= \frac{E}{2} \left(1 - i \frac{\kappa_1}{\kappa_2}\right) e^{(i\kappa_1 + \kappa_2)a} \end{aligned} \quad (11)$$

After inserting the value of C and D in equation (7) and (8) and dividing them by A we get

$$1 + \frac{B}{A} = \frac{E}{A} e^{i\kappa_1 a} \left[\cosh(\kappa_2 a) - i \frac{\kappa_1}{\kappa_2} \sinh(\kappa_2 a) \right] \quad (12)$$

$$1 - \frac{B}{A} = \frac{E}{A} e^{i\kappa_1 a} \left[\cosh(\kappa_2 a) + i \frac{\kappa_1}{\kappa_2} \sinh(\kappa_2 a) \right] \quad (13)$$

Solving equations (12) and (13) for $\frac{B}{A}$ and $\frac{E}{A}$

$$\begin{aligned} \frac{B}{A} &= -i \frac{\kappa_1^2 + \kappa_2^2}{\kappa_1 \kappa_2} \sinh(\kappa_2 a) \left[2 \cosh(\kappa_2 a) + i \frac{\kappa_1^2 + \kappa_2^2}{\kappa_1 \kappa_2} \sinh(\kappa_2 a) \right]^{-1} \\ \frac{E}{A} &= 2 e^{-i\kappa_1 a} \left[2 \cosh(\kappa_2 a) + i \frac{\kappa_1^2 - \kappa_2^2}{\kappa_1 \kappa_2} \sinh(\kappa_2 a) \right]^{-1} \end{aligned}$$

$$\text{Then Transmission probability, } T = \frac{|E|^2}{|A|^2} = 4 \left[4 \cosh^2(\kappa_2 a) + \left(\frac{\kappa_1^2 - \kappa_2^2}{\kappa_1 \kappa_2} \right)^2 \sinh^2(\kappa_2 a) \right]^{-1} \quad (14)$$

Since $\cosh^2(\kappa_2 a) = 1 + \sinh^2(\kappa_2 a)$ one can get in equation (14)

$$T = \left[1 + \frac{1}{4} \left(\frac{\kappa_1^2 - \kappa_2^2}{\kappa_1 \kappa_2} \right)^2 \sinh^2(\kappa_2 a) \right]^{-1} \quad (15)$$

Where $\left(\frac{\kappa_1^2 - \kappa_2^2}{\kappa_1 \kappa_2} \right)^2 = \left(\frac{V_B}{\sqrt{E(V_B - E)}} \right)^2 = \frac{V_B^2}{E(V_B - E)}$ Then

$$T = \left[1 + \frac{1}{4} \frac{V_B^2}{E(V_B - E)} \sinh^2 \left(\frac{a}{\hbar} \sqrt{2m(V_B - E)} \right) \right]^{-1} \quad (16)$$

For $E \ll V_B$

$$T \approx \frac{16E}{V_B} \left(1 - \frac{E}{V_B} \right) e^{-\frac{2a\sqrt{2m(V_B - E)}}{\hbar}} \approx e^{-2\kappa_2 z} \quad (17)$$

The solution of the equation inside a rectangular barrier in one dimension has the form:

$$\Psi = e^{\pm 2\kappa_2 z} \quad (18)$$

Here E is the energy of the state, and V_B is the potential in the barrier. For our case of STM we will consider only rectangular barrier. For the simple calculation, V_B is simply vacuum level; so for states in the Fermi level, $V_B - E$ is work function.

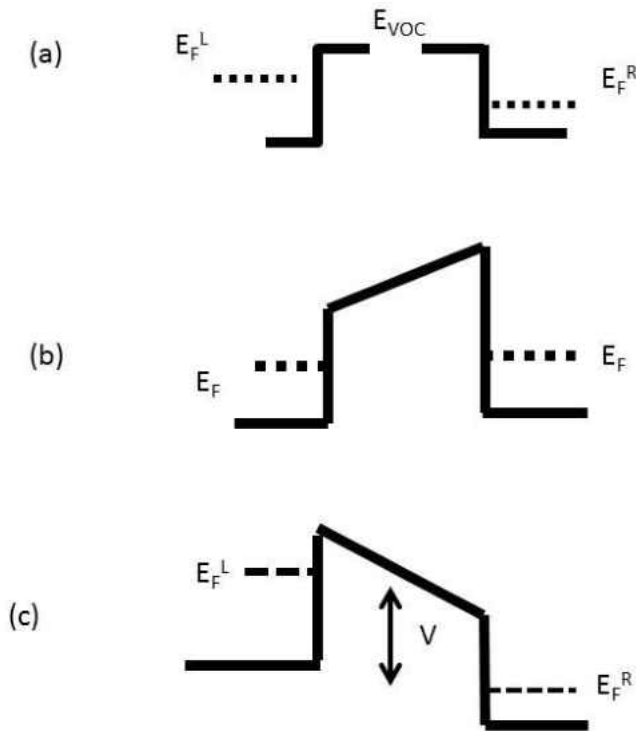


Figure 2.4: Potential for vacuum barriers for two electrodes. (a) Two non-interacting electrodes in between them is vacuum. Their Fermi level E_F differs by work function (E_F^R and E_F^L indicates Fermi level of right and left electrodes, respectively) (b) two electrodes are in electrical equilibrium so their Fermi level is same (c) A voltage is applied. There is a voltage drop, V across the gap (Fermi level differs by eV) work function difference and applied voltage

contribute to the field in the barrier. The arrow denotes the range of energy where tunneling can happen. At higher energy there is no electron to tunnel. At lower energy, there is no empty state to tunnel into.

With barrier width z , Transmission probability (Tunneling current) decays exponentially as

$$I \propto e^{-2kz} \quad (19)$$

The generalization of a real three dimensional surface is given below.

With the voltage difference, V across the gap, only the states within V above and below the Fermi level can contribute to the tunneling. With electrons in states within V below the Fermi level on the negative side tunneling into empty states above the Fermi level on the positive side.

As most work functions are around 4-5 eV from equation (19) we find that typically $2K \sim 2A^\circ$ [14]. Therefore, the tunneling current drops by nearly an order of magnitude for every $1A^\circ$ of vacuum between two electrodes. For keeping the current stable, requires very precise control of the position of electrodes, confining vibration less than an Armstrong.

2.3 Theory of Scanning Tunneling Spectroscopy (STS):

2.3.1 I (V) Spectroscopy:

By keeping the STM tip height fixed, we take the topographic image of the surface. To keep the current constant, STM electronics with the feedback loop adjusts the distance between the tip and the sample during this process; changes in the length of the z-piezo are recorded as the topographical image of the surface. For getting the I-V spectrum of the surface, at each point on the surface the STM electronics should ramp in an interval. Moreover, as long as the feedback circuit is closed, the tip always adjusts its position in order to keep the current constant. To shun this, we opened the feedback circuit so that for each lateral position, the tip stays at a constant z-position. Then at the corresponding voltage, a sudden increase or decrease in the I(V) curve is that electrons find or possible states to tunnel. The goal of I(V) curve is to determine the position of each state in the spectrum [7].

To explain I(V) spectroscopy in detail, we need to discuss some theoretical model. In the simplest model, the tunneling current is considered as the direct result of the density of states of

the sample and the tunneling rate. We assume that the tip has a constant density of state which will make our calculation a lot easier. Then current become proportional to:

$$I(V) \propto \int_0^{eV} \rho_s(E) T(E, eV) dE \quad (20)$$

where, ρ is the density of states of the sample at any energy E with respect to Fermi level. T is the transition probability between the tip and the substrate. We can write Transition Probability as:

$$T(E, eV) = e^{-2\kappa z} \quad (21)$$

$$\kappa = \sqrt{\frac{2m\phi^-}{\hbar^2} + K^2} \quad (22)$$

$$\phi^- = \frac{\phi_t + \phi_s}{2} - E + \frac{eV}{2} \quad (23)$$

where, ϕ_s and ϕ_t are work functions of sample and tip respectively. κ is called inverse decay length. Since electrons mainly use the Γ point to tunnel as long as there is a state at that point with the specified energy, we can assume $k \cong 0$. If so, κ is

$$\kappa \cong \sqrt{\frac{2m\bar{\phi}}{\hbar^2}}$$

We can roughly derive the tunneling current as:

$$dI/dV = \rho_s(E) T(eV, eV) + \int_0^{eV} \rho_s(E) \left(\frac{dT(E, eV)}{dV} \right) dE \quad (24)$$

Disregarding the second term, we see that derivative of tunneling current with respect to voltage is proportional to density of state of sample. But in its current form, the exponential functions $T(eV, eV)$ and $\frac{dT(E, eV)}{dV}$ overshadow spectral features. To avoid this problem, Feenstra [6] suggested to normalize differential conductance by dividing it to conductivity, I/V .

$$\text{LDOS} = \frac{dI/dV}{I/V} = \frac{\rho_s(E) + \int_0^{eV} \frac{\rho_s(E)}{T(eV, eV)} \frac{dT(E, eV)}{dV} dE}{\frac{1}{eV} \int_0^{eV} \frac{\rho_s(E)}{T(eV, eV)} T(E, eV) dE} \quad (25)$$

A careful analysis of the equation reveals that LDOS is proportional to surface density of states and dividing all the exponential functions somewhat cancels them out.

2.3.2 I(z) Spectroscopy:

This technique is based on the z dependence of the tunneling current [8]. When the tip is retracted from or approached to the surface the change in the tunneling current is recorded. At low sample bias, $\bar{\phi}$ can be approximated as from equation (23):

$$\bar{\phi} \cong \frac{\phi_t + \phi_s}{2}$$

Then the tunneling current becomes,

$$I(V) \propto T \int_0^{eV} \rho_s(E) dE \quad (26)$$

$$T = e^{-2\kappa z} \quad (27)$$

where T is transmission probability and κ is inverse decay length.

The derivative of the current with respect to z becomes

$$\frac{dI}{dz} \propto \frac{dT}{dz} \int_0^{eV} \rho_s(E) dE \quad (28)$$

The derivative of the current with respect to z becomes

$$\frac{dI}{dz} \propto \frac{dT}{dz} \int_0^{eV} \rho_s(E) dE \quad (29)$$

To simplify the equation above we can divide it by the current;

$$\frac{dI/dz}{I} = -2\kappa \cong -2\sqrt{\frac{2m\bar{\phi}}{\hbar^2}} \quad (30)$$

Equation (23) gives us an idea about average of tip and sample work function.

Chapter 3

IRIDIUM MODIFIED SILICON (001) SURFACE

3.1 Si (001) Surface:

Si (001) surface is generally used in the semiconductor industry. Silicon (Si) is a semiconductor whose atomic Number is 14 and mass is 28.085. The crystal structure is diamond cubic (space group: 227) with a lattice constant of 5.45 Å. Electron configuration: $1s^2 2s^2 2p^6 3s^2 3p^2$ with 4 electrons at its outermost shell. The s and p orbitals of the outermost shell hybridize and form $3sp^3$ orbitals. Therefore, each Si atom can make four bonds with its neighboring atoms. For the case of Si (001) surface, two of the bonds reach the level below and two of them reach the next level. By splitting along (001) surface, two bonds remain intact and other two bonds form a dangling bond (an unsatisfied valence on the immobilized atom). However, two dangling bonds per surface Si atom increases surface free energy and therefore the two Si atoms come together and form dimers. The dimerization leads to the formation of (2x1) unit cell on the surface.

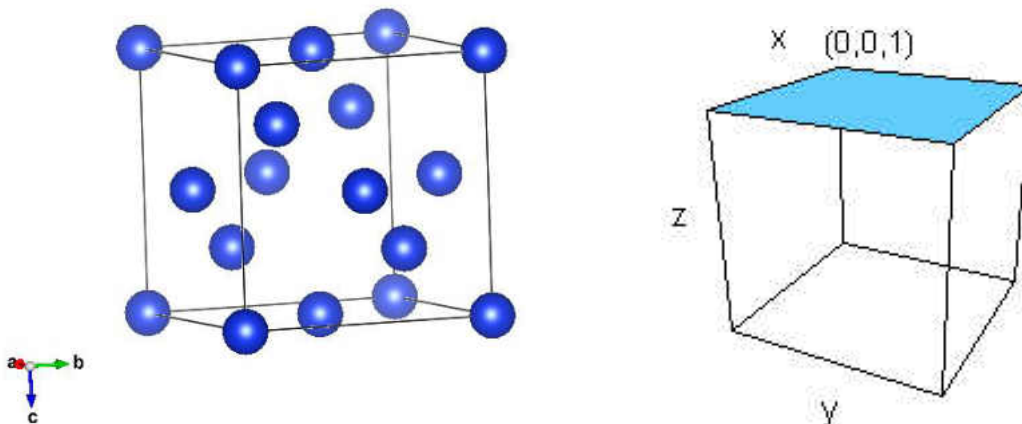


Figure 3.1: a) A Silicon Crystal , b) (001) surface

As Silicon has a Diamond Cubic structure, each terrace is perpendicular to the next. That's why (1x2) and (2x1) domains have been observed.

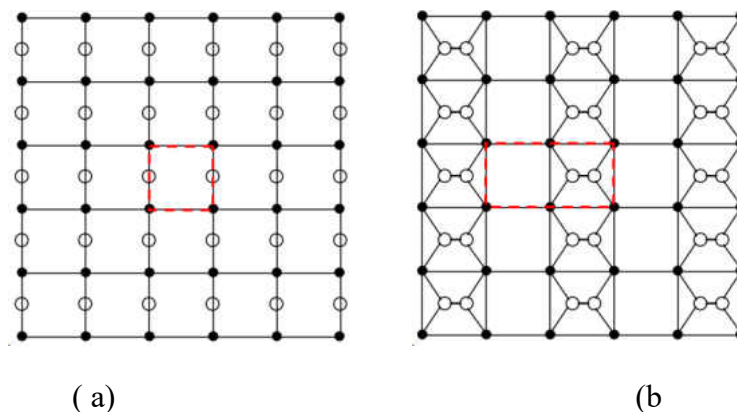


Figure.3.2: Top view of different Si (001) surface. White circles show atom in the surface layer while black circles show atom in the second layer but big white and small grey circles are used to show upward and downward buckled dimer atoms on the surface respectively. (a) The non reconstructed surface (b) (2×1) symmetric dimer reconstruction [11, 12]

3.1.1 Preparing the Sample

Samples were cut from nominally flat $76.2 \text{ mm} \times 0.38 \text{ mm}$, single side polished n-type (phosphorus doped) wafers. Then, we briefly washed the samples with isopropanol and dried them with blowing nitrogen gas. The samples were degassed extensively under ultra high vacuum. The samples were then flash annealed at 1250 C° . The quality of the clean Si(001) samples was checked and confirmed both with LEED and STM. Figure 3.1 shows a typical STM image of the surface.

After examining the sample surface, we decided that we will anneal the sample for a few times like six times to get our desired surface and after annealing we got a clean Si (001) surface. We got clean and smooth surface with a lot less defect. After getting image like above Figure 3.1, we decided to move to our next level experiment. As the sample is clean, nice with less impurity and defect, it was ready for further process and fabrication and very much suitable for Molecular Beam Epitaxy (MBE).

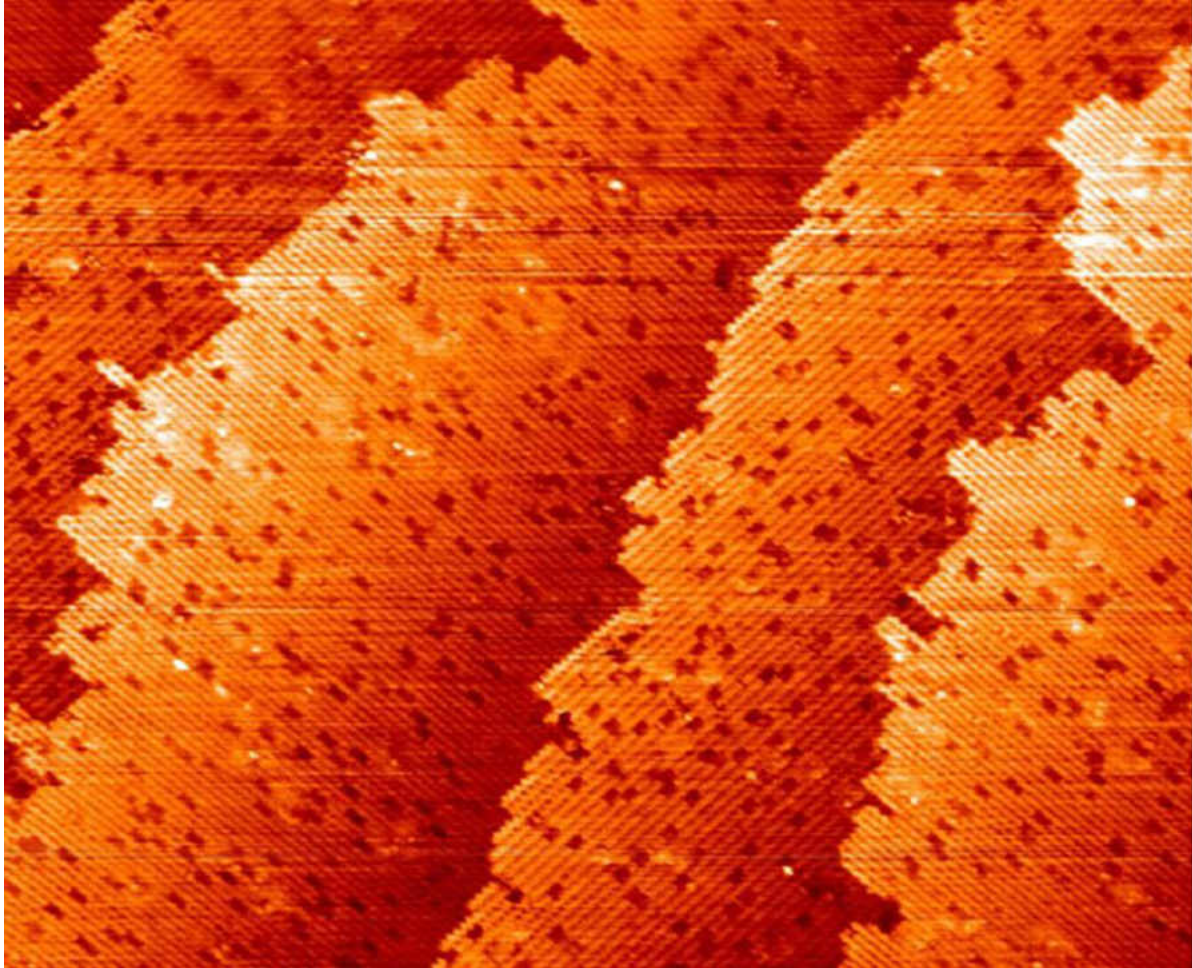


Figure 3.3: Zoomed Clean Si (001) surface taken in 75nm × 75nm frame with -1.0513V bias voltage and 0.4689 nA current

3.1.2 Experiment:

Ir was deposited over the clean Si(001) surface from a current heated Ir wire with a standard deposition rate of $2.8 \times 10^{-4} nm s^{-1}$. The deposition rate was measured and calibrated with the help of Auger spectrometer. After deposition at room temperature, the sample was annealed at 700 °C. The LEED and STM measurements showed that, if annealed at 700 °C, Ir-modified Si(001) surface turned into relatively small, irregular-shaped Ir-silicide terraces that exhibit a $p(2 \times 2)$ LEED pattern. If the sample was annealed above 800 °C, these terraces disappeared and Si(001) surface started to come back. The nanowires on the terraces stretch along [110] directions similar to dimer rows of a clean Si(001) surface. [1] This indicates that the morphology of Si(001) surface directly influences the structure of these nanowires. The surface has Ir rich terraces surrounded by Si(001) terraces with high density of vacancy line defects. STM images of Ir-silicide nanowires have bright and dark regions along a nanowire. (Figure 3.4) The height difference between these bright and dark regions is about $0.7 \pm 0.1 \text{ \AA}$. In addition to that the relative positions of high and low regions of two neighboring nanowires are in registry leading the formation of the $p(2 \times 2)$ LEED pattern [12].

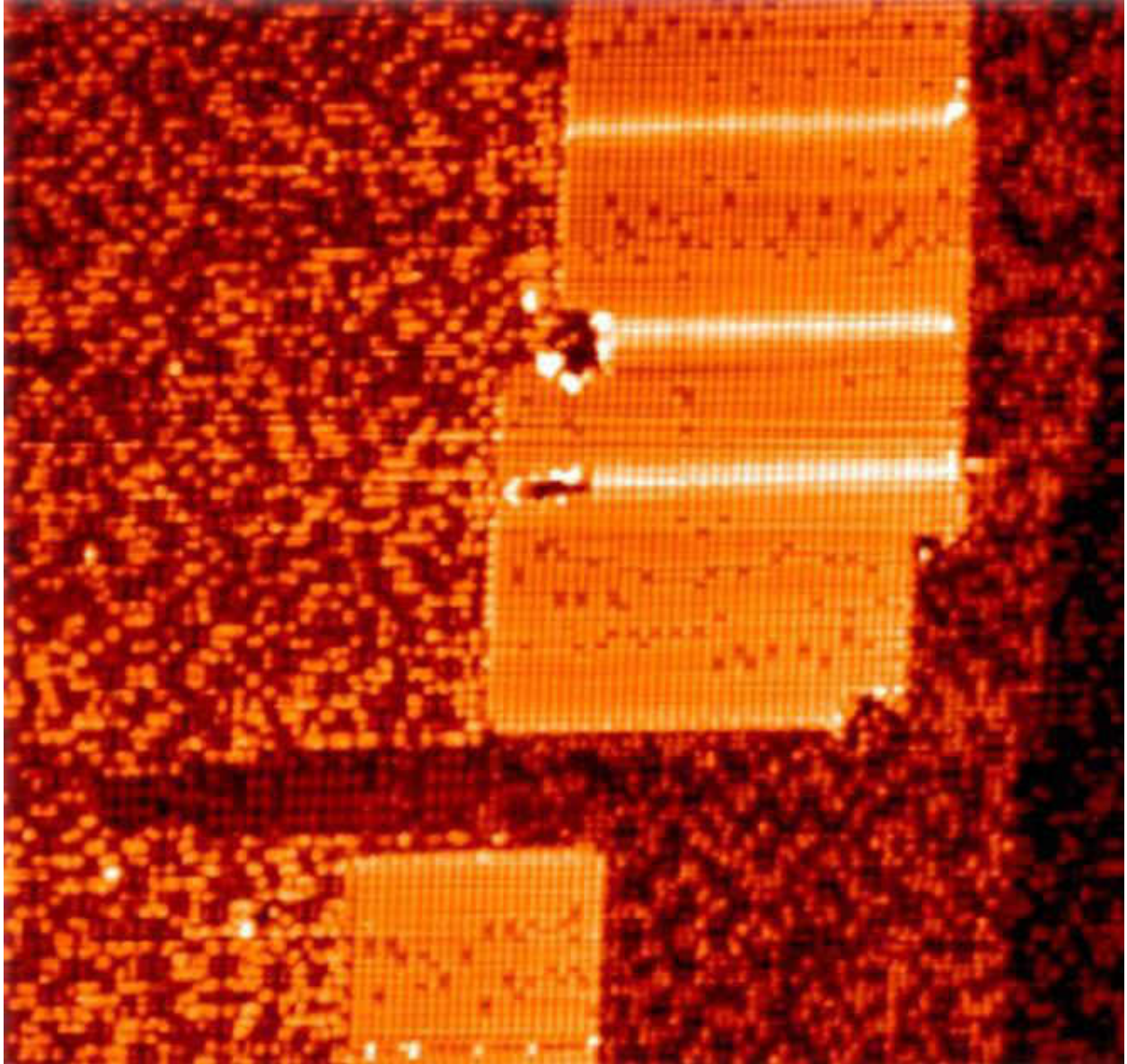


Figure 3.4: Zoomed in frame of 30nm × 30nm with -2.093 V biasing voltage and 0.3899nA tunneling current. Islands got much bigger, organized and visible.

3.2 Data Analysis

In the Second stage of the research, I analyzed the data. This stage consists of data analysis of the STM images and spectroscopy. From STM images I measure height, width and length of the Ir islands. From I-V spectroscopy data I calculate Local Density of state (LDOS) and from I-z spectroscopy data I calculate Inverse decay length (k) and surface work function.

3.2.1 Measurement of height, length and width

First, I analyzed the width and length of nanowire and arranged them according to monolayer. For this experiment we deposited from 0.25 monolayer to 0.5 monolayer exposure (Table: 1)

Table 1: Table of Width, Length, Height, W/L ratio and Coverage of Iridium Islands

Length(nm) L	Width(nm) W	Height(nm)	W/L	Coverage	Integer Long Length	Integer Short Length
16.653	6.576	0.32100	2.5323	0.25	17	7
9.104	7.289	0.23829	1.24900	0.25	9	7
6.544	11.77	0.20599	0.55590	0.25	7	12
4.357	5.340	0.14057	0.81590	0.25	4	5
4.953	4.953	0.26781	0.7372	0.25	5	7
4.86	9.920	0.33371	0.48990	0.25	5	10
3.33	4.982	0.33371	0.66840	0.25	3	5
6.013	8.448	0.34195	0.71170	0.25	6	8
5.334	9.434	0.36255	0.56540	0.25	5	9
5.162	9.413	0.33371	0.54839	0.25	5	9
4.475	10.228	0.32959	0.43752	0.25	4	10
4.894	10.246	0.22659	0.47760	0.25	5	10
4.483	8.217	0.31311	0.54550	0.25	4	8
7.453	6.587	0.32135	1.13140	0.25	7	7
7.422	10.512	0.05100	0.70600	0.25	7	11
38.17	6.648	0.09060	5.74157	0.25	38	7
11.881	20.366	0.18540	0.58337	0.25	12	20
3.96	27.440	0.33536	0.14430	0.25	4	27
13.06	13.060	0.38974	0.45690	0.25	13	29
13.023	17.256	0.26821	0.75460	0.25	13	17

6.21	6.2100	0.11500	0.32438	0.5	6	19
5.701	12.0680	0.18952	0.47240	0.5	6	12
5.858	11.6670	0.23454	0.50200	0.5	6	12
5.483	8.8460	0.13156	0.61980	0.5	5	9
5.315	19.9830	0.20599	0.26590	0.5	5	20
5.35	9.3840	0.11984	0.57010	0.5	5	9
3.302	11.7690	0.34607	0.28050	0.5	3	12
7.517	14.6300	0.19776	0.51380	0.5	8	15
5.263	14.1260	0.13146	0.37257	0.5	5	14
3.579	5.5130	0.24307	0.64910	0.5	4	6
6.047	11.6250	0.10712	0.52010	0.5	6	12
3.493	7.1250	0.17304	0.49020	0.5	3	7
5.381	11.5060	0.30457	0.46760	0.5	5	12
5.561	5.8730	0.14420	0.94680	0.5	6	6
4.348	7.5840	0.13596	0.57330	0.5	4	8
3.784	5.4130	0.13650	0.69900	0.5	4	5
50.276	37.140	0.20599	1.35360	0.5	50	37
45.362	35.210	0.71274	1.28830	0.5	45	35
44.445	53.4180	0.13596	0.83200	0.5	44	53
28.603	20	0.15244	1.43015	0.5	29	20

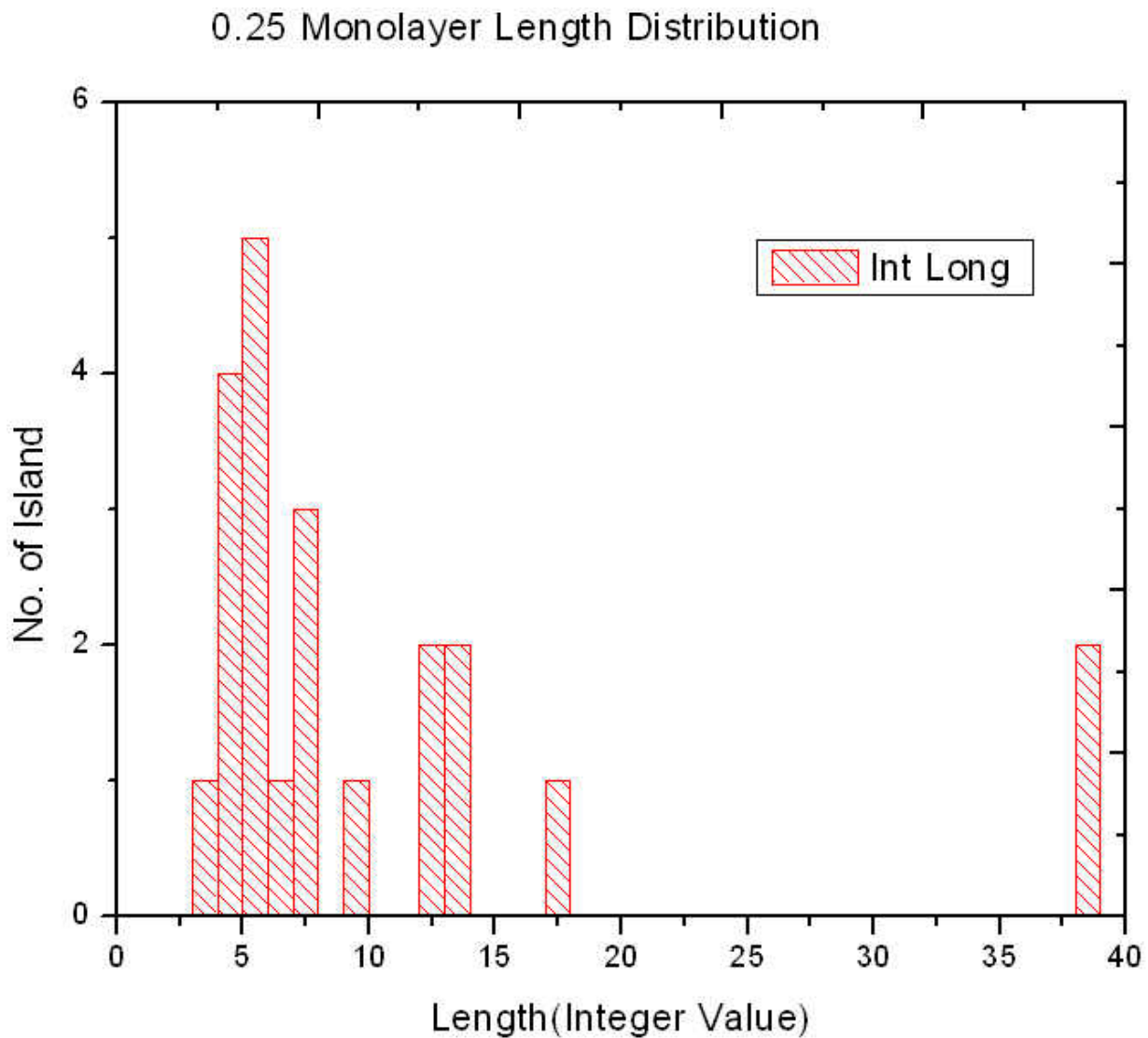


Figure 3.5: Length vs Number of Island histogram for 0.25 ML Islands

When we analyzed the nanowire islands by plotting length Vs number of island histogram, we see that majority of the islands are densely populated within the length of 3-8 nm and maximum frequency distribution is 5nm. I presumed that 3 nm is the minimum length to form a nanowire island for the case of 0.25 ML Islands (Figure 3.5). For the case of statistical analysis, we see Average length is 10.13nm, with standard deviation 9.77, minimum length is 3nm and maximum is 38nm.

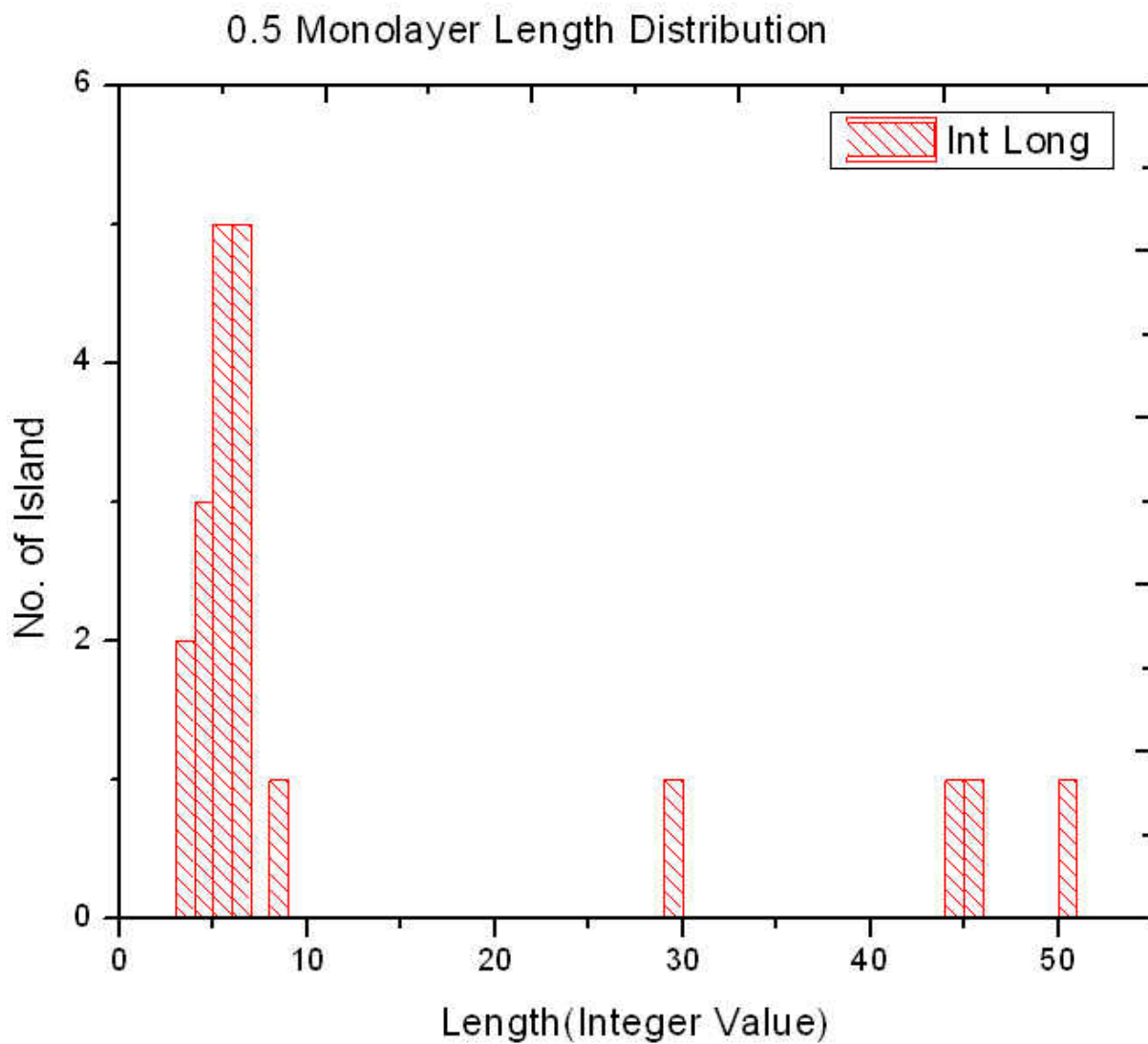


Figure 3.6: Length vs Number of Island histogram for 0.5 ML Islands

Then we analyzed for 0.5 ML Islands (Figure 3.6). For the case of 0.5 ML we see maximum islands concentrated in 3-10 nm regions and its minimum length is 3 nm and maximum frequency distribution is 5nm and 6nm. For statistical analysis, average length is 11.41 with Standard deviation: 6.93, minimum length 5nm and maximum length is 29nm.

For width distribution for 0.25 ML we see that maximum islands are in the region of 5nm-13nm region and minimum width is 5nm and maximum frequency distribution is 7nm (Figure 3.7) . Average width is 11.4nm with standard deviation is 6.93, minimum width 5nm and maximum is 29nm.

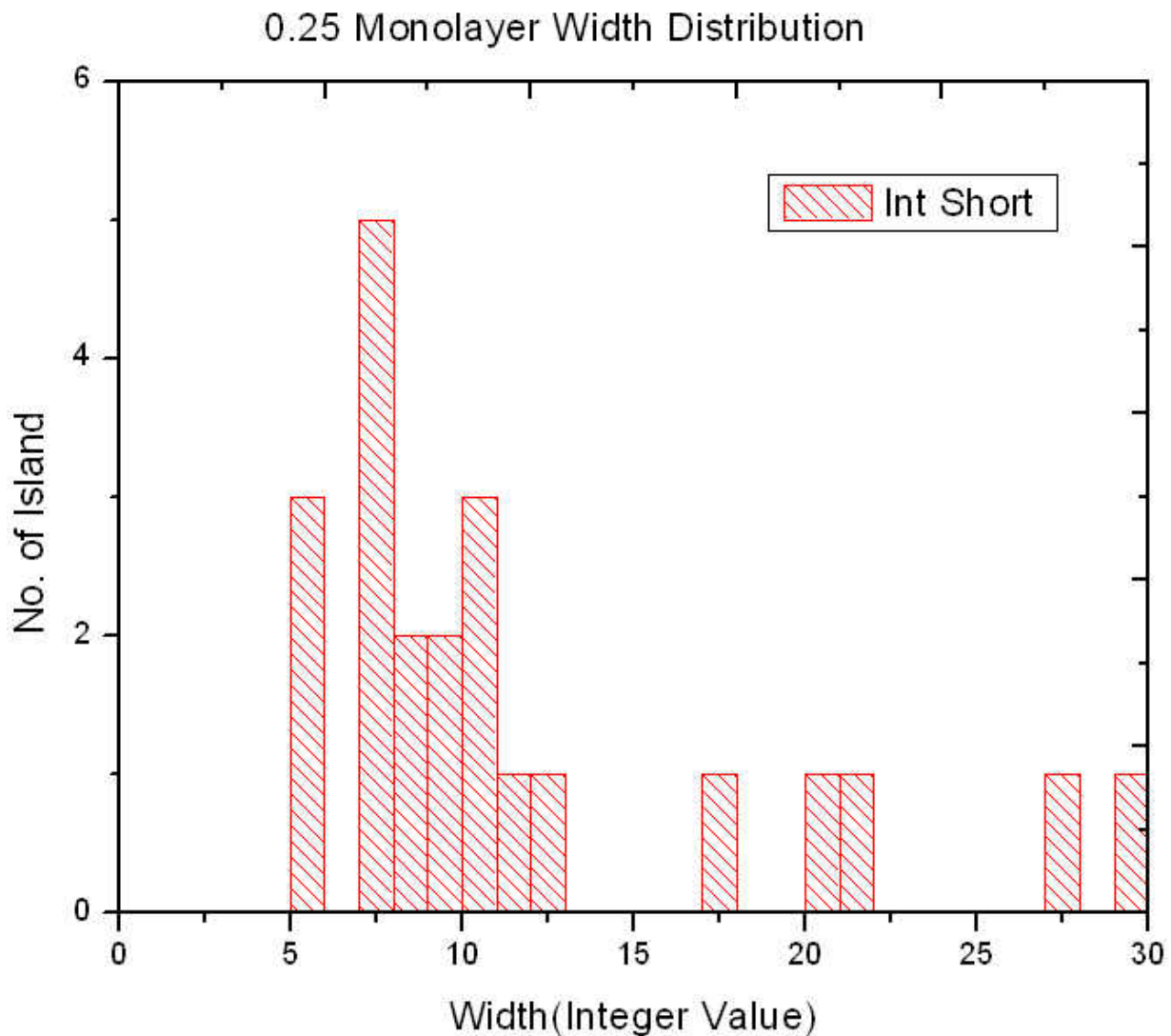


Figure 3.7: Width vs number of Island histogram for 0.25 ML Islands.

For 0.5 ML width distribution, maximum islands are concentrated in 5-15 nm regions and minimum width is 5nm and maximum frequency distribution is 11nm. Average width is 12.45nm with standard deviation is 15.6, minimum width is 3 nm and maximum is 50nm (Figure 3.8).

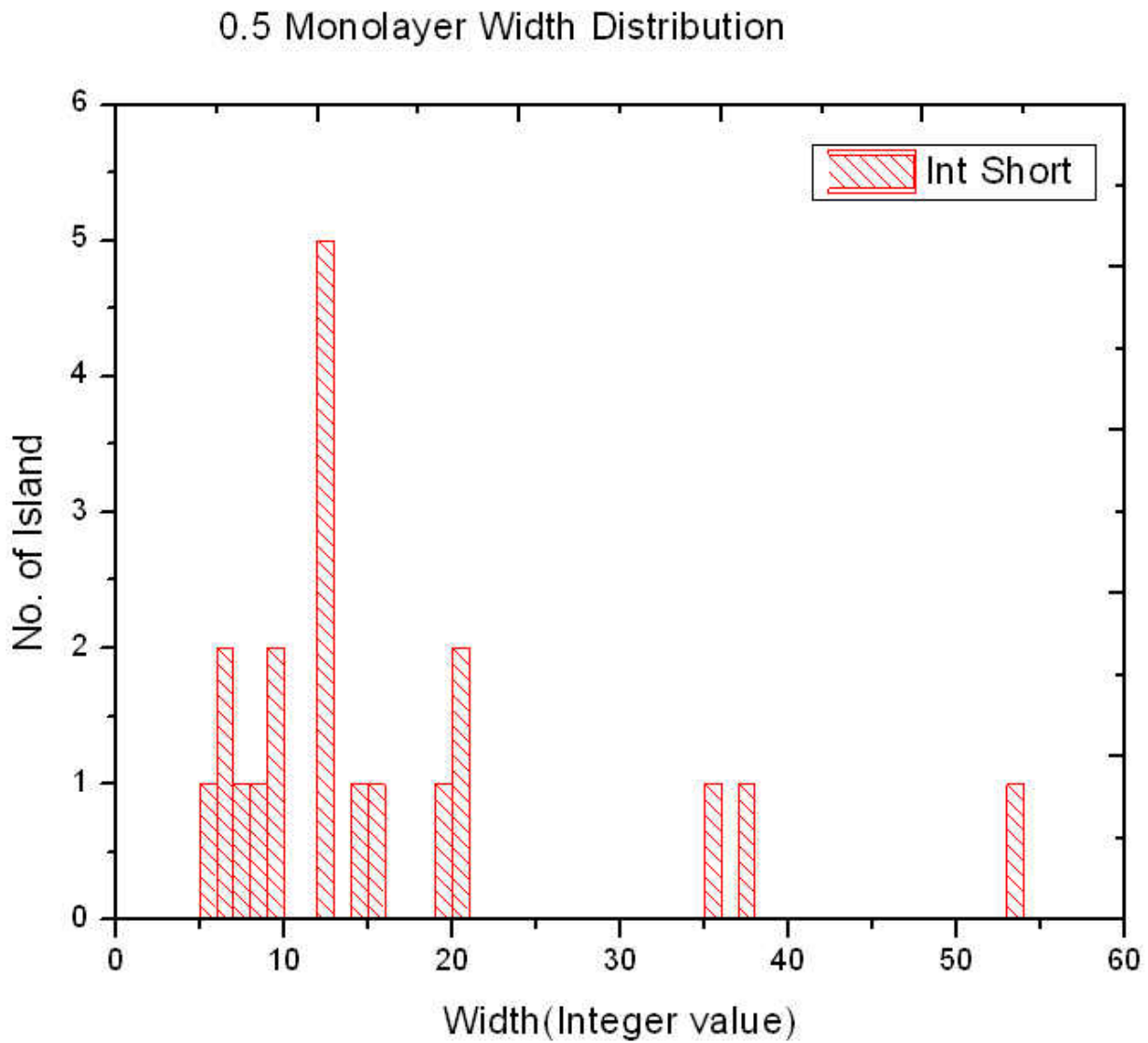


Figure 3.8: Width vs number of Island histogram for 0.5 ML Islands

We also did analysis of height distribution For the case of 0.25 ML we see maximum islands have height in between 0.3 to 0.35 nm. Average height is 0.26nm with Standard deviation: 0.09, minimum is 0.05nm and maximum is 0.38nm .

For the case of 0.5 ML Ir we see Maximum Island has height from 0.1 to 0.2 nm. Average height is 0.206nm with standard deviation is 0.13, minimum is 0.107nm and maximum is 0.71nm.

3.2.2 Correlation Analysis

Correlation analysis is concerned with change in model response due to variance of the parameter value. For our case, we consider width and length of the islands and disregard height as do not show any difference [20]. We analyzed length and width distribution to see correlation which is shown in Table:2.

Table:2 Correlation Analysis

Sample Type	Function $z= wl$	Covariance	σ_z^2 (nm ²)	Uncorrelated $\sigma_z^2=W^2\sigma_L^2+L^2\sigma_W^2$ (nm ²)	Correlated $\sigma_z^2=W^2\sigma_L^2+L^2\sigma_W^2+2\hat{W}\hat{L}\sigma_{WL}$ (nm ²)
All Islands	$z= wl$	19.782	18228	10811	16757
0.5 ML	$z= wl$	8.5731	12172	8305	13304
0.25 ML	$z= wl$	0.3239	3763	3791	3836

After analyzing the statistical data we see that islands are correlated with their length and width. Calculating variance of area, we see that it is closer to the correlated variance rather than uncorrelated variance indicating that there is a correlation between width and length of an islands. For the case of 0.25 ML coverage, we see that the distinction between correlated/uncorrelated is not obvious, indicating that at higher surface coverage the correlation between width and area becomes more relevant.

3.2.2 I(V) Spectroscopy:

The position of states can be determined by I(V) spectroscopy. It is considered that tunneling current and tunneling rate are directly depend on density of states of the sample. After preparing several samples and analyzing all data we got curve like Figure 3.9.

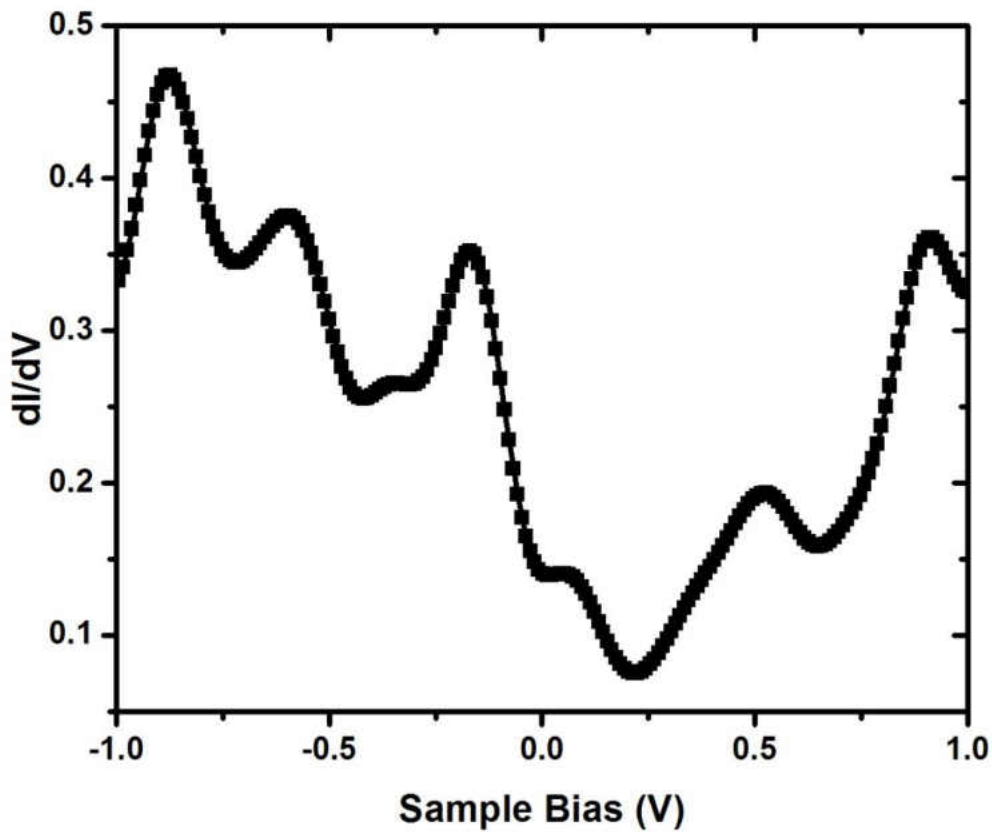


Figure.3.9: dI/dV vs sample bias voltage curve from I(V) spectroscopy data on Ir silicide terrace

Two peaks are visible at $V=0.5$ and 0.9 which are above Fermi level and other three peaks approximately at -0.2 , -0.6 and -0.9 V are below Fermi level. The state at -0.2 V crosses the Fermi level indicating the metallic nature of the Ir-silicide terraces. In order to find out the origins of the peaks, we need to investigate with ab-initio type calculations.

3.2.3 I(z) Spectroscopy:

After plotting the different values of I(z) spectroscopy, we saw that each curve has a little difference in their slopes. So we plotted $\ln I$ vs. z curve of all the spectroscopy and we saw each curve superimpose each other and their slope is -12.32626 (Figure.3.10). From the graph we can assume that work function of all three surface will have a little bit or just negligible difference.

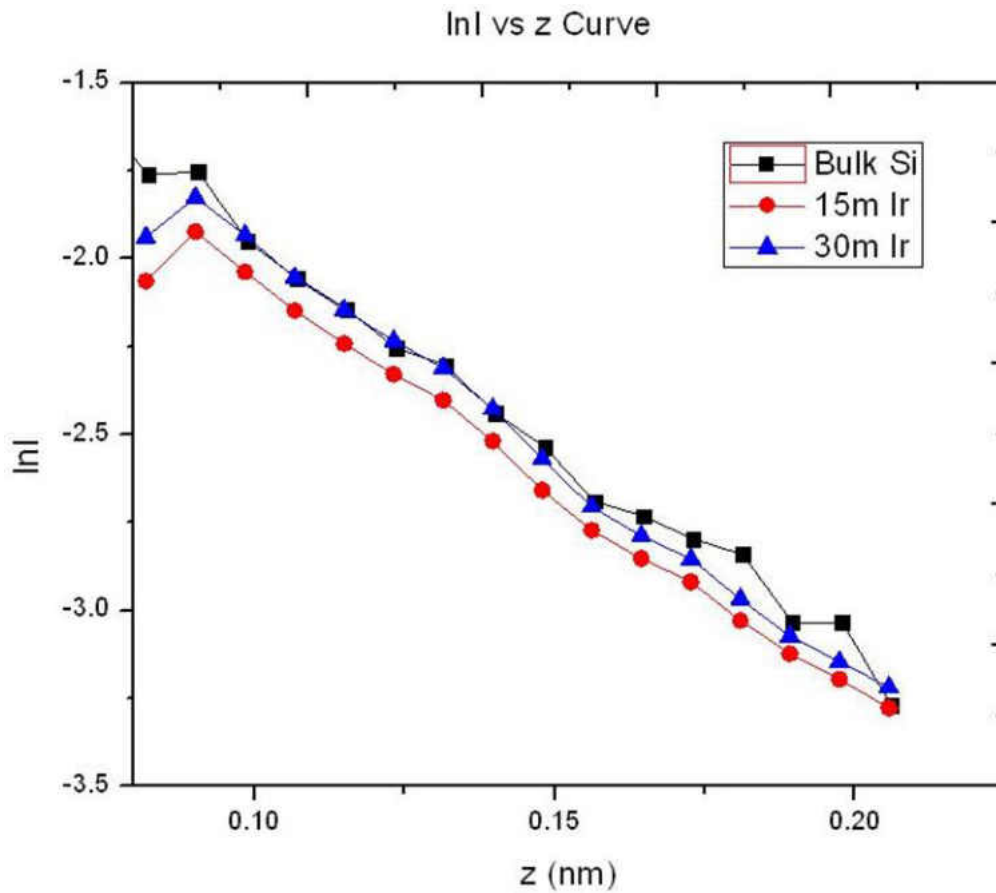


Figure 3.10: $\ln I$ vs. z curve of Bulk Si(001), 0.25ML Ir diffused and 0.5 ML Ir diffused Si(001) surface.

I(z) spectroscopy showed us some interesting data. We can see from Figure 3.10 that all the slopes are same. For all cases inverse decay length is same and after calculating work function of the surface we see there are a little bit difference between Bulk Si and Deposited two surfaces.

When we checked our work function with M.Wittmer, P. Oelhafen, K.N. Tu "Chemical reaction and Schottky-barrier formation at the Ir/Si interface", Physical Review B, Vol. 35, No.17 [13] , the difference is negligible. So the experimental data are with good agreement with M.Wittmer et al [13].

Chapter 4

CONCLUSION

The primary aim of this thesis is to fabricate Iridium nanowire on Silicon (001) surface. In the second chapter we represent our fabricated thin Ir nanowire on Si(001) surface image which took a lot of processing steps and preparation. After fabrication, we see some difference in islands forming if we change the deposition time. For longer deposition time we see larger islands and number of nanowire increased.

In chapter three, we analyzed the nanowire islands in terms of height, length and width and we saw that depositing Iridium for longer time, islands merged with each other to form larger islands. Majority of the islands are within the length of 3-8 nm and maximum frequency distribution is 5nm for 0.25 ML deposition and I presumed that 3 nm is the minimum length to form a nanowire island for the case of 0.25 ML Islands. For the case of 0.5 ML we see maximum islands concentrated in 3-10 nm regions and its minimum length is 3 nm and maximum frequency distribution is 5nm and 6nm. After that we analyzed statistically width and length of the islands after several calculation we see that correlation result match with length-width variance which denotes there is a correlation between length and width.

Along that we did some spectroscopy analysis. From $I(V)$ spectroscopy we got dI/dV vs V curve. We took spectroscopy along the nanowire and also along the sides. From that curve we saw there is a little bit bandgap in the curve which denotes the surface is acting like a semiconductor and the curve consists of several picks which confirms availability of several density of states.

Not only $I(V)$ spectroscopy but also $I(z)$ spectroscopy is performed. After some measurement we got the work function of the surface and we compare our result in several conditions like bulk Si and diffused for 15 and 30 minutes and see a little bit difference in the work function of the surface which is negligible. We also compared our result with some previous work [13] and see a little bit difference in work function which is almost negligible. So the experiment result is in nice agreement with the previous work.

All the spectroscopic analysis and fabrication were done previously [13] but island statistical analysis is not done. And correlation analysis is also new way to analyze nanowire from which we can know about the growth and formation of nanowire. So island statistical analysis and correlation analysis put a novelty in this thesis.

The origin of the peaks from I (V) spectroscopy curve is not analyzed. This study is needed to be done by Ab-initio calculation. Other study on bonding and hybridization need to be done by Density Functional Theory (DFT) calculation. I hope these studies will be done in near future.

References

- [1] Oncel N, van Houselt A, Huijben J, Hallback A S, Gurlu O, Zandvliet H J W and Poelsema B 2005 *Phys. Rev. Lett.* **95** 116801
- [2] van Houselt A, Oncel N, Poelsema B and Zandvliet H J W 2006 *Nano Lett.* **6** 1439
- [3] van Hove M A, Koestner R J, Stair P C, Biberian J P, Kesmodel L L, Bartos I and Somorjai G A 1981 *Surf. Sci.* **103** 189
- [4] Zhang Y P, Yang L, Lai Y H, Xu G Q and Wang X S 2004 *Appl. Phys. Lett.* **84** 401
- [5] Okino H, Matsuda I, Hobara R, Hosomura Y, Hasegawa S and Bennett P A 2005 *Appl. Phys. Lett.* **86** 233108
- [6] Kida A, Kajiyama H, Heike S, Hashizume T and Koike K 1999 *Appl. Phys. Lett.* **75** 540
- [7] Binnig G, Rohrer H. 1982. Scanning tunneling microscopy. *Helv. Phys. Acta* **55**:726–35
- [8] Joseph A. Stroscio, William J. Kaiser, Scanning Tunneling Microscopy, Academic Press Inc, 1993
- [9] C. Julian Chen, Introduction to Scanning Tunneling Microscopy, Oxford University Press, 1993
- [10] Zettili Nouredine “Quantum Mechanics Concepts and Application” Wiley, 2nd Edition
- [11] Charles B. Duke, “Semiconductor Surface Reconstruction: The Structural Chemistry of Two-Dimensional Surface Compounds”, *Chem. Rev.* **1996**, *96*, 1237–1259
- [12] D.J Chadi, *Phys. Rev letters*, **59**, *15*, 1987
- [13] M. Wittmer, P. Oelhafen, K.N. Tu “Chemical reaction and Schottky-barrier formation at the Ir/Si interface”, *Physical Review B*, Vol. **35**, No. *17*
- [14] Feenstra R.M., Stroscio J.A., Fein A.P., *Surface Science*, **181**, 295-306, 1987
- [15] Tersoff J., Hamann D., *Phys. Rev B*, **31**, 805, 1985
- [16] Tersoff J., Hamann D., *Phys. Rev B*, **50**, 1998, 1983

- [17] Harold J W Zandvliet, Arie van Houselt, Annual Review of Analytical Chemistry, 2, 37-55, 2009
- [18] Oncel Nuri, Masters Thesis, University of Twente, 2004
- [19] Neaman, Fundamental of Semiconductor Physics, Oxford Press
- [20] S.M.Sze, Fundamental of Semiconductor Physics, Oxford Press
- [21] H. J.W. Zandvliet, Reviews of Modern Physics 72, 593, 2000.